Embodying Quasi-Passive Modal Trotting and Pronking in a Sagittal Elastic Quadruped

Calzolari, Davide; Santina, Cosimo Della; Giordano, Alessandro M.; Schmidt, Annika; Albu-Schaffer, Alin

DOI
10.1109/LRA.2023.3249631

Publication date
2023

Document Version
Final published version

Published in
IEEE Robotics and Automation Letters

Embodying Quasi-Passive Modal Trotting and Pronking in a Sagittal Elastic Quadruped

Davide Calzolari, Cosimo Della Santina, *Senior Member, IEEE*, Alessandro M. Giordano, Annika Schmidt, and Alin Albu-Schäffer, *Fellow, IEEE*

***Abstract*—Animals rely on the elasticity of their tendons and muscles to execute robust and efficient locomotion patterns for a vast and continuous range of velocities. Replicating such capabilities in artificial systems is a long-lasting challenge in robotics. By taking advantage of a pitch dynamics decoupling spring potential, this work aims to provide design rules and a control strategy to generate dynamic, efficient locomotion patterns in quadrupeds moving in a sagittal plane. We rely on nonlinear modal theory, which provides the tools to characterize continuous families of efficient oscillations in nonlinear mechanical systems. We provide simulations of an elastic quadruped showing that the proposed solution can robustly excite efficient locomotion patterns under non-ideal conditions.**

***Index Terms*—Legged robots, natural machine motion, passive walking.**

I. Introduction

INSPIRED by the animal's muscle-skeletal system, researchers have built robots that include elastic elements in their design [1], [2], [3], [4]. The aim is to reproduce the high level of efficiency and robustness displayed by animals while executing periodic tasks - like locomotion [5]. Indeed, it has been experimentally demonstrated that the principle of exploiting elasticity, through the storage and release of energy to perform a designed motion, leads to higher efficiency and robustness, and improved robot control [6], [7], [8]. Yet, taking advantage of this elasticity has proven to be a quite challenging model-based design and control problem [6].

Researchers have devoted much attention to solve the task for simplified yet representative models, or templates [9]. Particularly relevant is the so-called spring loaded inverted pendulum (SLIP) [10], [11]. These theoretical results yielded relevant experimental results, by embedding these template models in complex robotic systems either through control [12], [13] or design [11], [14]. Efficient locomotion patterns can also arise in more complex carefully designed robots called passive walkers [15], [16]. Yet, these solutions suffer a major drawback: limited versatility. Indeed, locomotion patterns are isolated solutions which cannot be modulated to obtain - for example - different locomotion speeds. We believe that an alternative solution can be found in eigenmanifold theory [17], which shows that continuous families of nonlinear autonomous oscillations can be prolonged from equilibria of nonlinear mechanical systems. Each oscillation - or mode in an Eigenmanifold - corresponds to a different energy level. Exciting nonlinear modes of an elastically actuated leg led to swing-in-place and vertical jump motions in [18] and [19], respectively. The embodiment of a hopping in-place mode into a legged system was presented in [20]. Additionally, [21] has shown the existence and stability of passive bounding gaits for a range of speeds, while [22], [23] have proven the existence of continuous families of efficient gaits in a variation of the SLIP model. There, the gaits were found by satisfying periodicity constraints via numerical continuation. Finally, with [24], we have proposed a template model called P-SLIP that can generate continuous families of quasi-passive gaits[1] when combined with a closed loop control strategy that excite s its nonlinear modes. In the same work, we have applied the strategy for experimental forward hopping with an elastic leg. The advantage of using nonlinear modes lies in the fact that they are an intrinsic property of a mechanical system: modes can be straightforwardly analyzed, and they can be excited via relatively simple controllers [25], [26]. Although promising, these results are still limited to relatively simple mechanical systems, thus leaving open the question if modal locomotion generalizes to higher dimensional articulated systems. So far, the only validation of nonlinear modes with complex mechanical systems is [27], which however deals with oscillations in industrial manipulators and not locomotion. The goal of the present work is to make a step towards answering this question by showing that P-SLIP's nonlinear modes can be embedded in a quadruped moving in the sagittal plane. The main idea is to generate quasi-passive gaits by embedding nonlinear modes in the double support phase, in combination with planning of the attack configuration in the flight phase. More specifically,

Manuscript received 19 October 2022; accepted 8 February 2023. Date of publication 27 February 2023; date of current version 9 March 2023. This letter was recommended for publication by Associate Editor M. Focchi and Editor A. Kheddar upon evaluation of the reviewers' comments. This work was supported by European Research Council (ERC) through the European Union's Horizon 2020 Research and Innovation Programme under Grant 835284. *(Corresponding author: Alessandro M. Giordano.)*

Davide Calzolari, Alessandro M. Giordano, Annika Schmidt, and Alin Albu-Schäffer are with the Department of Informatics, Technical University of Munich, 85748 Garching, Germany, and also with the Institute of Robotics and Mechatronics, German Aerospace Center, 82234 Weßling, Germany (e-mail: davide.calzolari@dlr.de; Alessandro.Giordano@dlr.de; annika.schmidt@dlr.de; Alin.Albu-Schaeffer@dlr.de).

Cosimo Della Santina is with the Institute of Robotics and Mechatronics, German Aerospace Center, 82234 Weßling, Germany, and also with the Cognitive Robotics Department, Delft University of Technology, 2628 CD Delft, The Netherlands (e-mail: cosimodellasantina@gmail.com).

This letter has supplementary downloadable material available at https://doi.org/10.1109/LRA.2023.3249631, provided by the authors.

Digital Object Identifier 10.1109/LRA.2023.3249631

[1]With "quasi-passive" we indicate that part of the nominal gait can be performed completely passively, while some actuation is utilized supplementary to handle disturbances and to drive the system on the desired oscillation.

we contribute to the state of the art in efficient locomotion with elastic articulated quadrupeds[2] with the following:

i) A strategy for selecting elastic potentials to yield nonlinear modes useful for locomotion in sagittal elastic quadrupeds whose legs have negligible mass (Section III).
ii) The extension of the planning and control architecture introduced in [24] from a single leg to a quadrupedal robot (Sections IV-B and V-B).
iii) A critical analysis of the features and limitations of the approach, based on simulations under non-ideal conditions including impacts, friction losses, and model mismatch (Section VI).

II. Derivation of the Reduced-Order Model

Our methods are broadly applicable to sagittal elastic quadrupeds with lightweight non-redundant legs. This section introduces the model of this family of robots, and presents a convenient reduced representation of their dynamics, which we will later employ as the base for our derivations.

A. Full Order Model

Consider a generic quadrupedal robot endowed with an elastic potential U_{k}, and constrained to the sagittal plane. The robot consists of a floating base main body, or trunk, with legs attached to it. Let $\boldsymbol{\zeta} = [\boldsymbol{x}_{\mathrm{b}}^{\mathrm{T}}, \boldsymbol{q}^{\mathrm{T}}]^{\mathrm{T}} \in \mathbb{R}^n$, where $\boldsymbol{x}_{\mathrm{b}} = \begin{bmatrix} x, & z, & \phi \end{bmatrix}^{\mathrm{T}} \in \mathbb{R}^3$ are the trunk's CoM position and pitch angle, and $\boldsymbol{q} \in \mathbb{R}^{n_{\mathrm{j}}}$ denotes the joint angles of the legs. Using the Lagrangian formalism, the full-order sagittal dynamics is described by [23]

$$\begin{bmatrix} \boldsymbol{M}_{\mathrm{b}} & \boldsymbol{M}_{\mathrm{bq}} \\ \boldsymbol{M}_{\mathrm{bq}}^{\mathrm{T}} & \boldsymbol{M}_{\mathrm{q}} \end{bmatrix} \ddot{\boldsymbol{\zeta}} + \boldsymbol{c}(\boldsymbol{\zeta}, \dot{\boldsymbol{\zeta}}) + \boldsymbol{g}(\boldsymbol{\zeta}) + \begin{bmatrix} \boldsymbol{0} \\ \frac{\partial U_{\mathrm{k}}(\boldsymbol{q})}{\partial \boldsymbol{q}} \end{bmatrix} = \begin{bmatrix} \boldsymbol{0} \\ \boldsymbol{\tau} \end{bmatrix} + \boldsymbol{J}_{\mathrm{c}}(\boldsymbol{\zeta})^{\mathrm{T}} \boldsymbol{\lambda} \,, \tag{1}$$

where $\boldsymbol{M}_{\mathrm{b}} = \mathrm{diag}(m, m, I_{\mathrm{b}})$ is the inertia matrix of the trunk, $\boldsymbol{M}_{\mathrm{q}} \in \mathbb{R}^{n_{\mathrm{j}} \times n_{\mathrm{j}}}$ the inertia of the legs, $\boldsymbol{M}_{\mathrm{bq}} \in \mathbb{R}^{3 \times n_{\mathrm{j}}}$ the inertia couplings, $\boldsymbol{c} \in \mathbb{R}^n$ collects the Coriolis and centrifugal forces, U_{k} is the spring potential, $\boldsymbol{g} \in \mathbb{R}^n$ the gravity vector, $\boldsymbol{\tau} \in \mathbb{R}^{n_{\mathrm{j}}}$ represents the generalized leg actuation forces, $\boldsymbol{J}_{\mathrm{c}}$ is the contact Jacobian, and $\boldsymbol{\lambda}$ are the contact forces. We assume that the feet are the only contact points, and no slipping or sliding can occur. When a foot strikes the ground, there is an instantaneous change in velocity

$$\dot{\boldsymbol{\zeta}}^{+} = (\boldsymbol{I}_n - \boldsymbol{M}^{-1}\boldsymbol{J}_{\mathrm{c}}^{\mathrm{T}}(\boldsymbol{J}_{\mathrm{c}}\boldsymbol{M}^{-1}\boldsymbol{J}_{\mathrm{c}}^{\mathrm{T}})^{-1})\dot{\boldsymbol{\zeta}}^{-} \,, \tag{2}$$

where $\boldsymbol{I}_j$ is the $j \times j$ identity matrix, $\boldsymbol{M}$ is the inertia matrix of (1), and $(\cdot)^{-}$ and $(\cdot)^{+}$ indicate the velocities at the instants before and after the impact, respectively. If a leg is on the ground, the contact forces $\boldsymbol{\lambda}$ are calculated through the unilateral constraints, and can be explicitly expressed by

$$\boldsymbol{\lambda} = -(\boldsymbol{J}_{\mathrm{c}}\boldsymbol{M}^{-1}\boldsymbol{J}_{\mathrm{c}}^{\mathrm{T}})^{-1}\left(\boldsymbol{J}_{\mathrm{c}}\boldsymbol{M}^{-1}\left(\boldsymbol{c}+\boldsymbol{g}+\begin{bmatrix}\boldsymbol{0}\\ \frac{\partial U_{\mathrm{k}}}{\partial \boldsymbol{q}} - \boldsymbol{\tau}\end{bmatrix}\right) + \dot{\boldsymbol{J}}_{\mathrm{c}}\dot{\boldsymbol{\zeta}}\right). \tag{3}$$

The joint coordinates are grouped into $\boldsymbol{q} = [\boldsymbol{q}_{\mathrm{st}}^{\mathrm{T}}, \boldsymbol{q}_{\mathrm{fl}}^{\mathrm{T}}]^{\mathrm{T}}$, where $\boldsymbol{q}_{\mathrm{st}}$ denotes the joints of the legs in contact with the ground, while $\boldsymbol{q}_{\mathrm{fl}}$ of the legs not in contact.

[2]These systems are also labeled in many other ways, e.g., "articulated soft quadrupeds" or "compliant legged quadrupeds".

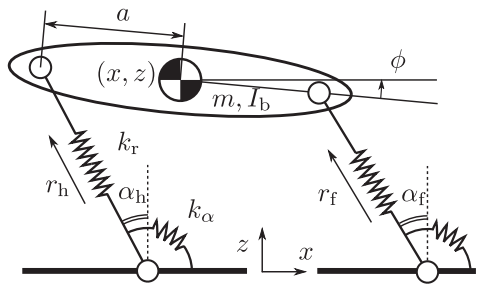

Fig. 1. Attachment of springs for potential design during double support. In a real system, the potential forces are realized by springs collocated at the joints and/or between robot links. The distance between the feet is $2a$.

B. Reduced-Order Model

Consider the following conditions

C 1: The legs have negligible mass and inertia, i.e., $\boldsymbol{M}_{\mathrm{q}} \to 0, \boldsymbol{M}_{\mathrm{bq}} \to 0$.

C 2: There are three possible locomotion phases: double support (one hind foot and one front foot in contact), single support (one foot in contact), and flight (no ground contact).

C 3: When in contact with the ground, the inverse kinematics of the trunk coordinates is solvable in closed-form, i.e., $\exists f_{\mathrm{ik}} : \mathbb{R}^3 \to \mathbb{R}^n$, *such that* $\boldsymbol{q}_{\mathrm{st}} = f_{\mathrm{ik}}(\boldsymbol{x}_{\mathrm{b}})$.

C1 implies that there is no loss of kinetic energy at impacts, thus (2) simplifies to $\dot{\boldsymbol{\zeta}}^{+} = \dot{\boldsymbol{\zeta}}^{-}$. As a consequence, C1 leads to a conservative system. Moreover, $\boldsymbol{c}(\boldsymbol{\zeta}, \dot{\boldsymbol{\zeta}}) \to 0$. Substituting (3) in the trunk dynamics of (1), and considering C1 and C3, leads to the simplified 3 DoF sagittal dynamics

$$\boldsymbol{M}_{\mathrm{b}}\ddot{\boldsymbol{x}}_{\mathrm{b}} + \boldsymbol{g}(z) = \frac{\partial f_{\mathrm{ik}}(\boldsymbol{x}_{\mathrm{b}})}{\partial \boldsymbol{x}_b}^{\mathrm{T}} \left(-\frac{\partial U_{\mathrm{k}}(\boldsymbol{q}_{\mathrm{st}})}{\partial \boldsymbol{q}_{\mathrm{st}}} + \boldsymbol{\tau}_{\mathrm{st}}\right). \tag{4}$$

This reduced-order model is mathematically equivalent to a free-floating trunk affected by the projected active spring and actuation forces, as the one shown in Fig. 1.

C. Convenient Formulation

We consider an alternative and more convenient choice of coordinates. We also take the opportunity to make explicit the hybrid nature of model, that we omitted in the previous subsection for the sake of space. It consists of the three continuous-time dynamic models defined in C2. The phases and the transition guards are reported in Fig. 2.

1) Double Support Phase (Stance Phase): During this phase, both feet are in contact with the ground. Let $\boldsymbol{p} = [\alpha_{\mathrm{h}}, r_{\mathrm{h}}, \alpha_{\mathrm{f}}, r_{\mathrm{f}}]^{\mathrm{T}} \in \mathbb{R}^4$ denote the polar and radial coordinates of the hind and front legs (see Fig. 1). We position the reference frame such that both feet are placed at a distance a from its origin. When the robot is in the upright configuration the legs are perpendicular to the ground (i.e. $\alpha_{\mathrm{h}} = \alpha_{\mathrm{f}} = 0$).

The system constitutes a closed-chain kinematic structure with 3 DoF. Thus, the coordinates $\boldsymbol{p}$ can be expressed as function of $\boldsymbol{x}_{\mathrm{b}}$ in closed-form, i.e., $\boldsymbol{p} = \boldsymbol{h}(\boldsymbol{x}_{\mathrm{b}})$

$$\begin{bmatrix}\alpha_{\mathrm{h}}\\ r_{\mathrm{h}}\\ \alpha_{\mathrm{f}}\\ r_{\mathrm{f}}\end{bmatrix} = \begin{bmatrix} -\arctan(s_{\mathrm{x,h}}/s_{\mathrm{z,h}}) \\ \sqrt{s_{\mathrm{x,h}}^2 + s_{\mathrm{z,h}}^2} \\ -\arctan(s_{\mathrm{x,f}}/s_{\mathrm{z,f}}) \\ \sqrt{s_{\mathrm{x,f}}^2 + s_{\mathrm{z,f}}^2} \end{bmatrix}, \quad \begin{aligned} s_{\mathrm{x,h}} &= x + a(1-\cos(\phi)),\\ s_{\mathrm{z,h}} &= z - a\sin(\phi)),\\ s_{\mathrm{x,f}} &= x - a(1-\cos(\phi)),\\ s_{\mathrm{z,f}} &= z + a\sin(\phi)). \end{aligned} \tag{5}$$

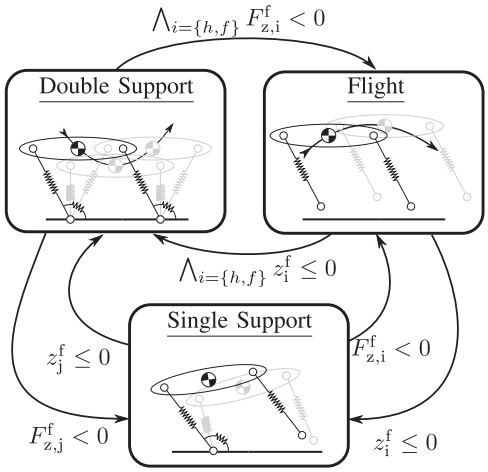

Fig. 2. The three phases of the reduced order model: double support - both feet in contact, single support - one of the feet in contact, and flight - no ground contact. The transition guard conditions of the hybrid model are reported. The feet vertical positions during flight and single support are calculated as $z^{\mathrm{f}}_{\mathrm{h,f}} = z \mp a \sin\phi - r_{\mathrm{atk}} \cos\alpha_{\mathrm{atk}}$.

The Jacobian of the coordinate transformation follows

$$\dot{\boldsymbol{p}} = \boldsymbol{H}(\boldsymbol{x}_{\mathrm{b}})\dot{\boldsymbol{x}}_{\mathrm{b}}, \quad \boldsymbol{H}(\boldsymbol{x}_{\mathrm{b}}) = \frac{\partial \boldsymbol{h}(\boldsymbol{x}_{\mathrm{b}})}{\partial \boldsymbol{x}_b} \ . \tag{6}$$

The trunk is under the effect of gravity, springs forces, and joint actuation. Therefore, the trunk's double support dynamics expressed in trunk coordinates is

$$\boldsymbol{M}_{\mathrm{b}}\ddot{\boldsymbol{x}}_{\mathrm{b}} + \boldsymbol{g}(z) + \frac{\partial U_{\mathrm{k}}(\boldsymbol{h}(\boldsymbol{x}_{\mathrm{b}}))}{\partial \boldsymbol{x}_{\mathrm{b}}} = \boldsymbol{H}(\boldsymbol{x}_{\mathrm{b}})^{\mathrm{T}}\boldsymbol{u}_{\mathrm{p}} \ , \tag{7}$$

where $\boldsymbol{u}_{\mathrm{p}} \in \mathbb{R}^4$ represents the generalized leg actuation forces in $\boldsymbol{p}$ space. The trunk coordinates coincide with the position of the system's CoM; $\boldsymbol{M}_{\mathrm{b}}$ is constant in these coordinates.

Since the legs of the model have no mass, the tangential and normal ground reaction forces $\boldsymbol{F}^{\mathrm{f}}_{\mathrm{xz}} \in \mathbb{R}^4$ at the feet are

$$\boldsymbol{F}^{\mathrm{f}}_{\mathrm{xz}} = \begin{bmatrix} \boldsymbol{F}^{\mathrm{f}}_{\mathrm{xz,h}} \\ \boldsymbol{F}^{\mathrm{f}}_{\mathrm{xz,f}} \end{bmatrix} = \boldsymbol{J}_{\mathrm{xp}}(\boldsymbol{p})^{-\mathrm{T}} \left(\boldsymbol{f}_k + \boldsymbol{u}_{\mathrm{p}}\right) \ , \tag{8}$$

where $\boldsymbol{f}_k$ are the spring forces acting on the legs, and $\boldsymbol{J}_{\mathrm{xp}}(\boldsymbol{p}) \in \mathbb{R}^{4\times4}$ is the Jacobian mapping $\dot{\boldsymbol{x}}^{\mathrm{f}} = \boldsymbol{J}_{\mathrm{xp}}(\boldsymbol{p})\dot{\boldsymbol{p}}$, being $\boldsymbol{x}^{\mathrm{f}} \in \mathbb{R}^4$ the Cartesian coordinates of the feet.

2) Flight Phase: When in flight, the system follows a ballistic trajectory and conserves its momentum

$$\boldsymbol{M}_{\mathrm{b}}\ddot{\boldsymbol{x}}_{\mathrm{b}} + \boldsymbol{g}(z) = 0, \quad \boldsymbol{p} = \boldsymbol{p}_{\mathrm{atk}} \ . \tag{9}$$

Since the legs have no mass, we assume that the joint angles can be controlled during the flight phase to the desired attack configuration $\boldsymbol{p}_{\mathrm{atk}}$ without affecting the trunk motion.

3) Single Support: During a single support phase a single foot is in contact with the ground. Therefore, the system becomes an under-actuated serial robotic chain. Within the scope of gait design concept of this work, the nominal motion does not entail the single support phase. Thus, for the sake of space, we do not discuss this phase further. Note however that this phase is considered in the simulations of Sections V and VI.

III. Embedding Nonlinear Modes

We introduce an arrangement of springs that results in an elastic potential that does not induce rotations when the trunk is parallel to the ground. This property of the resulting nonlinear modes is exploited to construct locomotion patterns for trotting and pronking with modulable speed based on natural oscillations.

A. Proposed Choice of Elastic Potential

The proposed choice of coordinates for the reduced order mode allows for a straightforward definition of a convenient elastic potential

$$U_{\mathrm{k}}(\boldsymbol{p}) = \frac{1}{2}k_\alpha\left(\alpha_{\mathrm{h}}^2 + \alpha_{\mathrm{f}}^2\right) + \frac{1}{2}k_{\mathrm{r}}\left((r_{\mathrm{h}} - r_0)^2 + (r_{\mathrm{f}} - r_0)^2\right) \ . \tag{10}$$

where k_{r} and k_α are the stiffnesses of the two radial and torsional springs, respectively. The former are attached between the shoulders and the feet, the latter between the leg and the ground - as shown in Fig. 1. Note that the springs presented in this reduced model are virtual. In a real system, the actual potential forces are realized by physical mechanical springs collocated at the joints and/or between distant robot links. Finally, r_0 is the rest length of the radial springs.

B. Pitch Dynamics Decoupling

The elastic potential yields a decoupled rotational dynamics of the trunk for $\phi = 0$ during double support. Consider the pitch component in (7), $I_b\ddot{\phi} + \tau_{\mathrm{k},\phi} = \frac{\partial \boldsymbol{h}(\boldsymbol{x}_{\mathrm{b}})}{\partial \phi}^{\mathrm{T}}\boldsymbol{u}_{\mathrm{p}}$ where $\tau_{\mathrm{k},\phi}$ is the net torque acting on the trunk around the CoM due to the springs

$$\begin{aligned}\frac{\tau_{\mathrm{k},\phi}}{a} = &+\frac{\sin(\alpha_{\mathrm{h}} - \phi)}{r_{\mathrm{h}}}\tau_{\mathrm{k,h}} - \frac{\sin(\alpha_{\mathrm{f}} - \phi)}{r_{\mathrm{f}}}\tau_{\mathrm{k,f}} \\ &- \cos(\alpha_{\mathrm{h}} - \phi)f_{\mathrm{k,h}} + \cos(\alpha_{\mathrm{f}} - \phi)f_{\mathrm{k,f}} \ .\end{aligned} \tag{11}$$

Here, $\tau_{\mathrm{k,j}} = -k_\alpha\alpha_{\mathrm{j}}$ and $f_{\mathrm{k,j}} = -k_{\mathrm{r}}(r_{\mathrm{j}} - r_0)$ are the spring forces. For $\phi = 0$, (5) shows that a generic configuration of the trunk parallel to ground ($\boldsymbol{x}_{\mathrm{b}} = [x, z, 0]^{\mathrm{T}}$) is achieved only for $r_{\mathrm{h}} = r_{\mathrm{f}}$ and $\alpha_{\mathrm{h}} = \alpha_{\mathrm{f}}$. Then, in the subset of the configuration space where $\phi = 0$, the hind and front spring forces originating from (10) are equivalent, i.e., $\tau_{k,h} = \tau_{k,f}$, and $f_{k,h} = f_{k,f}$. It follows immediately that $\tau_{\mathrm{k},\phi} = 0$ in (11), i.e. the rotational dynamics is not excited. This implies that if the system is initialized at $\phi_0 = \dot{\phi}_0 = 0$, then for arbitrary $x_0, \dot{x}_0, z_0, \dot{z}_0$, the autonomous system evolutions of (7) suitable for passive locomotion (i.e., with $\boldsymbol{u}_{\mathrm{p}} = 0$) are fully described by

$$m\begin{bmatrix}\ddot{x} \\ \ddot{z}\end{bmatrix} - m\begin{bmatrix}0 \\ g\end{bmatrix} + \begin{bmatrix}\frac{\partial U_{\mathrm{k}}(\boldsymbol{x}_{\mathrm{b}})}{\partial x} \\ \frac{\partial U_{\mathrm{k}}(\boldsymbol{x}_{\mathrm{b}})}{\partial z}\end{bmatrix} = 0, \quad \phi \equiv \dot{\phi} \equiv 0 \ . \tag{12}$$

The oscillations that take place in the subspace described by (12) entails swinging motion of the trunk without rotation. This feature facilitates the creation of natural gaits and allows to devise a planning methodology. To show the existence of these oscillations, we use nonlinear modal analysis to characterize the family of natural oscillations that the model can perform as autonomous evolutions during double-support using the potential defined in (10).

C. Nonlinear Modes of the Reduced-Order Sagittal Model

When moving from linear mechanical systems to robots, the flat invariant collections of regular oscillations that we find in linear systems (eigenspaces) are curved into 2-dimensional invariant submanifolds embedded in the robot's state space (eigenmanifolds) [17]. Still, these objects collect infinite self-similar and hyper-efficient periodic orbits - one for each energy level.

An eigenmanifold $\mathfrak{M}$ for the present system can be represented as follows

$$\mathfrak{M} \simeq \Big\{(x,z,\phi,\dot{x},\dot{z},\dot{\phi}) \in \mathbb{R}^6 \mid \exists(\xi_{\mathrm{m}},\dot{\xi}_{\mathrm{m}}) \in \mathbb{R}^2 \\ \text{s.t. } (x,z,\phi) = X(\xi_{\mathrm{m}},\dot{\xi}_{\mathrm{m}}),\ (\dot{x},\dot{z},\dot{\phi}) = \dot{X}(\xi_{\mathrm{m}},\dot{\xi}_{\mathrm{m}})\Big\}, \tag{13}$$

where $(X,\dot{X}) : \mathbb{R}^2 \to \mathbb{R}^3 \times \mathbb{R}^3$ is the coordinate expressions of the natural embedding of $\mathfrak{M}$ into $\mathbb{R}^6$. The first argument of $(X,\dot{X})$ is called master variable ξ_{m}. We can define a retraction $\boldsymbol{\pi} : \mathbb{R}^3 \to \mathbb{R}$ from (x,z,ϕ) to ξ_{m}. All these functions encode the necessary information about the eigenmanifold geometry, and as such, they play an important role in the proposed control framework. In this work, we use polynomials to approximate $(X,\dot{X})$.

To carry out the nonlinear modal analysis, the spring forces must be sufficiently strong for the system to have an upright, stable equilibrium.

Since system (7) has 3 DoF, there are at least three eigenmanifolds, each one tangent to the eigenspaces of the linearized system [17]. One is the eigenmanifold collecting vertical oscillations which realize hopping in place motions $\{(x,z,\phi,\dot{x},\dot{z},\dot{\phi}) \in \mathbb{R}^6 \mid x \equiv 0,\ \dot{x} \equiv 0,\ \phi \equiv 0,\ \dot{\phi} \equiv 0\}$. In this special case, the tangency constraints can be solved without any approximation. This describes vertical oscillations in the z direction, governed by the modal dynamics $\ddot{z} = -g + 2k_{\mathrm{r}}(z - r_0)/m$, which can be used to implement in place hopping. Yet no forward motion can be obtained this way since no swinging of the main body is involved.

A second eigenmanifold collects the rotating and translating motions of the trunk. In general, for $\phi \neq 0$, the spring forces excite the whole state of the trunk, and the dynamics do not simplify like in the previous case.

A third Eigenmanifold is associated with swinging motions of the trunk, which are useful for constructing quasi-passive gaits. At the equilibrium configuration, this manifold is tangent to the eigenvector $\boldsymbol{v} = [1,0,0]^{\mathrm{T}}$. The resulting oscillations take place in the subspace described by (12), where $\phi = \dot{\phi} = 0$. The relevant nonlinear mode arising in this subspace corresponds to swing motions that do not involve or excite the trunk rotation, thanks to the designed potential. Since the system is symmetric, these oscillations generate either U-shaped or reversed U-shaped motions of the COM, depending on the system parameters. For this Eigenmanifold, a natural choice for the master variable ξ_{m} is x. Thus, the first elements of X and $\dot{X}$ are the identity. As examples, we report in Fig. 3 the swing motion manifold for the set of system parameters presented in the simulation section, together with examples of autonomous orbits for different energy levels. Furthermore, the swinging trajectories of the trunk corresponding to these orbits are depicted in Fig. 4. Similar trajectories would be achieved for other choices of the spring constants within the proposed family.

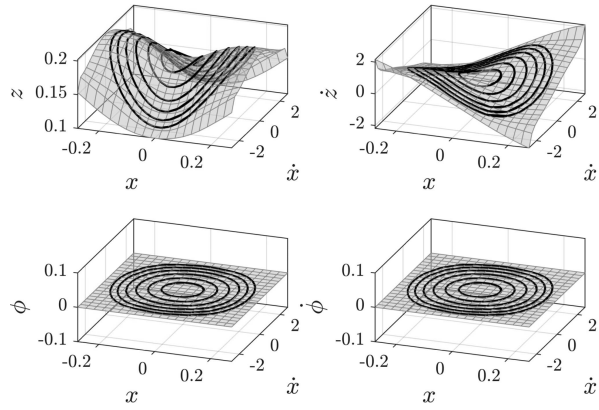

Fig. 3. Polynomial approximation of the Eigenmanifold (light gray) associated with swing motion of the mechanical system shown in Fig. 1, using the parameters discussed in the simulation section. Modal trajectories with constant energy levels are displayed with solid black lines. Thanks to the designed potential, the mode does not entail trunk rotations. The figure shows the nonlinear character of the Eigenmanifold - in comparison, a linear mode would result in a planar shape.

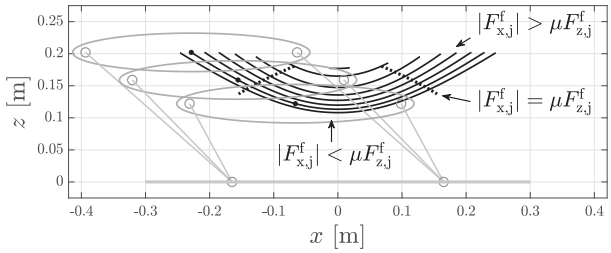

Fig. 4. Snapshots and trajectories of the trunk corresponding to autonomous orbits on the Eigenmanifold presented in Fig. 3 for a range of energy levels. This mode does not excite the rotation of the trunk, and the resulting swinging motion is exploited to build quasi-passive gaits. If we remove the constraint at the feet, the dotted lines delineate the border between the feasible and unfeasible motion (since a foot either loses contact or slides for $|F^{\mathrm{f}}_x| > \mu F^{\mathrm{f}}_z$, see footnote 3 below).

IV. Gait Planning Based on Nonlinear Modes

To generate quasi-passive gaits, the double support phases embedding nonlinear modes must be connected to the flight phases, such that the planned trajectory is a periodic orbit for the hybrid system. In [24], it is shown that this connection can be performed on the (attitude-constrained) P-SLIP model by designing the take-off and touch-down events and regulating the angle of attack during the flight phase. Here, we extend the idea to a more complex system with a non-fixed attitude and two legs, and we exploit the decoupling of the rotational dynamics. To this end, we introduce matching conditions for the state at the transition events, which ensure the desired behavior.

A. Matching Conditions

Let us define the touch down (TD) and take off (TO) related quantities belonging to k-th cycle with the superscript $(\cdot)^{\mathrm{k}}$. At each touch down the system should find itself on a modal trajectory

$$\begin{bmatrix} x^{\mathrm{k}}_{\mathrm{TD}} \\ z^{\mathrm{k}}_{\mathrm{TD}} \\ \phi^{\mathrm{k}}_{\mathrm{TD}} \end{bmatrix} \equiv X(x^{\mathrm{k}}_{\mathrm{TD}}, \dot{x}^{\mathrm{k}}_{\mathrm{TD}}) \ , \quad \begin{bmatrix} \dot{x}^{\mathrm{k}}_{\mathrm{TD}} \\ \dot{z}^{\mathrm{k}}_{\mathrm{TD}} \\ \dot{\phi}^{\mathrm{k}}_{\mathrm{TD}} \end{bmatrix} \dot{X}(x^{\mathrm{k}}_{\mathrm{TD}}, \dot{x}^{\mathrm{k}}_{\mathrm{TD}}) \ . \tag{14}$$

Note that the master variable here is $\xi_{\mathrm{m}} = x$, as described in Section III-C. Our design of a mode that entails swinging motion with constant body attitude simplifies the planning: on the chosen Eigenmanifold both $\phi^{\mathrm{k}}_{\mathrm{TD}}$ and $\dot{\phi}^{\mathrm{k}}_{\mathrm{TD}}$ are always zero, zero, and we only need to find the proper configuration $\boldsymbol{p}_{\mathrm{atk}}$ to perform the connection for each energy level (which relates to increasing forward speeds).

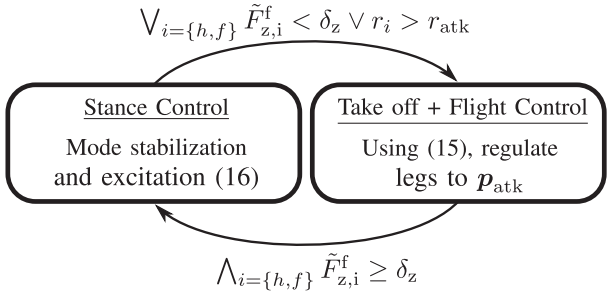

Fig. 5. A state machine manages the switching between the stance and the aerial controllers. $\tilde{F}^{\mathrm{f}}_{\mathrm{z,i}}$ denotes the estimated feet normal forces. The stance controller is activated only when both feet are in contact with sufficient force. If either the contact forces are insufficient or one leg stretches over r_{atk}, then the control system triggers the take off.

B. Attack Configuration Planning

The take off and touch down conditions are designed to exploit the feasible part of the modal oscillation[3] during double support and yield symmetrical double support phase. Given the Eigenmanifold $\mathfrak{M}$, and an energy level E^{d}, the reference attack configuration for the legs is calculated using the intersection of the modal trajectory with the constraints for feasibility of the ground reaction forces (GRF). The required state at touchdown is

$$\boldsymbol{x}^{\mathrm{d}}_{\mathrm{b,TD}} = \mathfrak{M}_{E(\boldsymbol{x}_{\mathrm{b}},\dot{\boldsymbol{x}}_{\mathrm{b}})=E^{\mathrm{d}}} \cap \{\, |F_{x,i}(\boldsymbol{x}_{\mathrm{b}})| \leq \mu F_{z,i}(\boldsymbol{x}_{\mathrm{b}}) \;, \quad i = \{h,f\}, \dot{z} < 0, \mathrm{sign}(x) = s_{\mathrm{x}} \} \;, \tag{15}$$

where $\mathfrak{M}_{E(\boldsymbol{x}_{\mathrm{b}},\dot{\boldsymbol{x}}_{\mathrm{b}})=E^{\mathrm{d}}}$ identifies the unique modal trajectory with energy level E^{d}, $F^{\mathrm{f}}_{\mathrm{x,i}}$ and $F^{\mathrm{f}}_{\mathrm{z,i}}$ are the tangential and normal contact forces due to the springs, respectively, at the hind and the front feet, μ is the friction coefficient between the feet and the ground, and $s_{\mathrm{x}} \in \{-1, 1\}$ is used to pick the desired direction of horizontal motion. We approximate the solution of (15) for $x^{\mathrm{d}}_{\mathrm{TD}}$ and $z^{\mathrm{d}}_{\mathrm{TD}}$ analytically, using polynomials. Fig. 6 presents an example of the approximations, while Fig. 4 depicts the solution with dotted lines against the modal trajectories within the studied energy range. By design, it always results $\phi^{\mathrm{d}}_{\mathrm{TD}} = 0$. During the flight phase, the legs are regulated to the desired attack configuration $\boldsymbol{p}_{\mathrm{atk}} = \boldsymbol{h}(\boldsymbol{x}^{\mathrm{d}}_{\mathrm{b,TD}})$. The mapping also provides the matching velocities $\dot{x}^{\mathrm{d}}_{\mathrm{TD}}$ and $\dot{z}^{\mathrm{d}}_{\mathrm{TD}}$ for each energy level. These velocities can be used to evaluate the speed of the gait for different energy levels, as shown in Fig. 7.

V. Control Architecture

The goal of the control architecture is to stabilize the gait at a desired energy level. The architecture consists of two controllers - one active during stance (both feet on the ground) and the other during flight (both feet in the air) - which are scheduled by a simple state machine (Fig. 5). The stance controller stabilizes the nonlinear mode to sustain a desired speed. The flight controller closes the hybrid orbit by regulating the angles of attack and radial lengths of the legs.

[3]The oscillations presented in Section III-C are evaluated with both feet rigidly attached to the ground. This can lead to oscillations that also require negative ground reaction forces, which are physically unrealizable once the foot is free to leave the ground. Here, we make use of the feasible part of these oscillations (see Fig. 4).

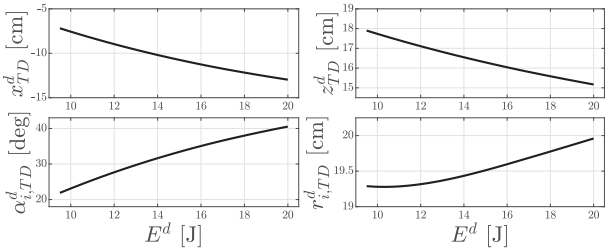

Fig. 6. State at touchdown (top plots) in function of the mechanical energy using modal information, with corresponding attack angles and leg lengths (bottom plots). To connect the stance phase modes for different speeds (i.e., different energy levels), a proper attack configuration is required.

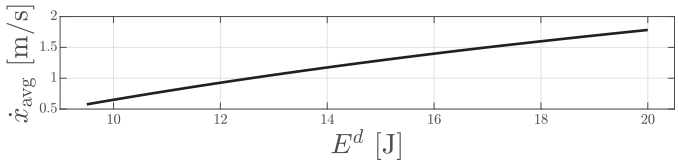

Fig. 7. Average forward speed for different energy levels.

A. Phase Detection

The transitions in the state machine in Fig. 5 correspond to the detection of transitions between the stance and flight phases. The detection is performed using thresholds on the estimated contact forces $\tilde{\boldsymbol{F}}^{\mathrm{f}}_{\mathrm{xz}}$, which can be obtained either via sensors at the feet or by projecting the forces acting on the legs. Whenever both forces $\tilde{F}^{\mathrm{f}}_{\mathrm{z,h}}$ and $\tilde{F}^{\mathrm{f}}_{\mathrm{z,f}}$ are higher than a threshold $\delta_z > 0$ for a minimum time interval, the state machine triggers the touch down event, and the control system switches to the stance controller. Similarly, when either $\tilde{F}_{\mathrm{z,h}}$ or $\tilde{F}_{\mathrm{z,f}}$ are below δ_z, or any leg stretches over the attack length r_{atk}, the take-off event is triggered.

B. Double-Support Mode Controller

The overall action of the mode controller is defined as [25]

$$\boldsymbol{u}_{\mathrm{p}} = \boldsymbol{H}(\boldsymbol{x}_{\mathrm{b}})^{+\mathrm{T}}_{W} \left(\boldsymbol{u}_{\mathrm{st}}(\boldsymbol{x}_{\mathrm{b}}, \dot{\boldsymbol{x}}_{\mathrm{b}}) + \boldsymbol{u}_{\mathrm{in}}(\boldsymbol{x}_{\mathrm{b}}, \dot{\boldsymbol{x}}_{\mathrm{b}}; E^{\mathrm{d}}) \right) \;, \tag{16}$$

where $(\cdot)^{+}_{W}$ indicates the generalized weighted pseudoinverse with weight $\boldsymbol{W} = \boldsymbol{J}^{-1}_{\mathrm{xp}} \boldsymbol{A} \boldsymbol{J}^{-\mathrm{T}}_{\mathrm{xp}}$, $\boldsymbol{A} = \mathrm{diag}(1, 1\mathrm{e}^{-3}, 1, 1\mathrm{e}^{-3})$ which minimizes the tangential forces to the ground, and

$$\boldsymbol{u}_{\mathrm{st}} = \boldsymbol{M}_{\mathrm{b}} \left(\boldsymbol{K} \left(\boldsymbol{x}_{\mathrm{b}} - X(\xi_{\mathrm{m}}, \dot{\xi}_{\mathrm{m}}) \right) + \boldsymbol{D} \left(\dot{\boldsymbol{x}}_{\mathrm{b}} - \dot{X}(\xi_{\mathrm{m}}, \dot{\xi}_{\mathrm{m}}) \right) \right) \;,$$

$$\boldsymbol{u}_{\mathrm{in}} = \gamma \boldsymbol{M}_{\mathrm{b}} \dot{X}(\xi_{\mathrm{m}}, \dot{\xi}_{\mathrm{m}}) (E^{\mathrm{d}} - E_{\mathrm{st}}(\boldsymbol{x}_{\mathrm{b}}, \dot{\boldsymbol{x}}_{\mathrm{b}})) \;, \tag{17}$$

with $\boldsymbol{K}, \boldsymbol{D} \in \mathbb{R}^{3\times3}$ the proportional and derivative, positive definite gain matrices, $\gamma > 0$ the energy regulation gain, and E_{st} the total mechanical energy during stance phase

$$E_{\mathrm{st}}(\boldsymbol{x}_{\mathrm{b}}, \dot{\boldsymbol{x}}_{\mathrm{b}}) = \frac{1}{2} \dot{\boldsymbol{x}}^{\mathrm{T}}_{\mathrm{b}} \boldsymbol{M}_{b} \dot{\boldsymbol{x}}_{\mathrm{b}} + mgz + U_{\mathrm{k}}(\boldsymbol{x}_{\mathrm{b}}) \;. \tag{18}$$

The objective of $\boldsymbol{u}_{\mathrm{st}}$ is to stabilize the swing eigenmanifold, i.e., $(\boldsymbol{x}_{\mathrm{b}}, \dot{\boldsymbol{x}}_{\mathrm{b}}) \to (X, \dot{X})$. The role of $\boldsymbol{u}_{\mathrm{in}}$ is to drive the system on the oscillation with the right amplitude by regulating the energy level, i.e., $E_{\mathrm{st}} \to E^{\mathrm{d}}$. In this way, a single swing-like modal orbit can be stabilized without relying on trajectory tracking controllers. Note that the overall controller is designed such that $\boldsymbol{u}_{\mathrm{p}} \to 0$ (hyper-efficient oscillation) when the system converges to the desired modal trajectory. This is possible because the

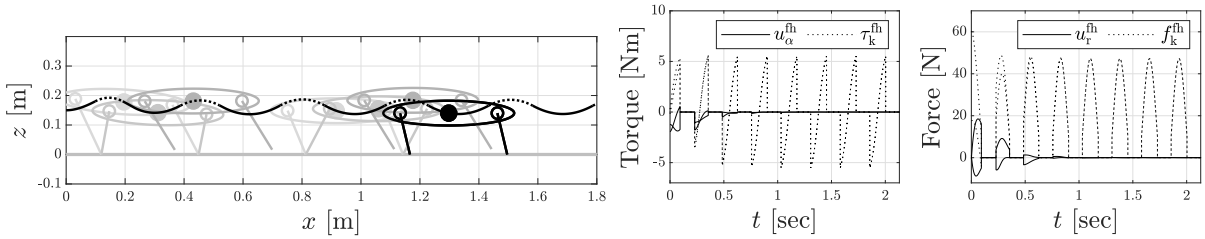

Fig. 8. Simulations of the reduced sagittal model controlled using the proposed approach and showing stable locomotion with target energy $E^d = 14\,\mathrm{J}$. The system is initialized outside of the mode with $z(0) = 0.15\,\mathrm{m}$, $\phi(0) = 0.2\,\mathrm{rad}$, $\dot{x}(0) = 1\,\mathrm{m/s}$, and $\dot{z} = \dot{\phi}(0) = 0$. Stance phase control inputs for both legs are reported with the corresponding spring contributions. After a few locomotion cycles, the trajectories evolve along the nonlinear mode, and the double-support control input converges to zero.

TABLE I
MODEL PARAMETERS FOR SIMULATION

m	I_b	k_α	k_r	a	r_0
$4.3\,\mathrm{kg}$	$0.1\,\mathrm{kg}\cdot\mathrm{m}^2$	$10\,\mathrm{Nm/rad}$	$650\,\mathrm{N/m}$	$16.5\,\mathrm{cm}$	$21\,\mathrm{cm}$

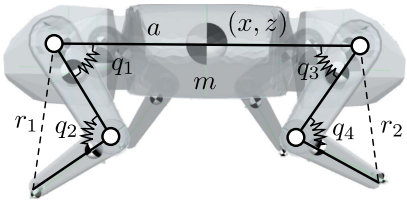

Fig. 9. Elastic quadruped model used for simulation with non-zero leg masses, joint friction and impact losses. In general, the springs forces are nonlinear, and couple multiple links. The contact between feet and ground has friction $\mu = 1$. The collision shapes of the feet are modeled via small spheres of 1 cm diameter. The ground contact stiffness and damping used for simulation are $k_\mathrm{p} = 10^6$ and $k_\mathrm{d} = 10$, respectively.

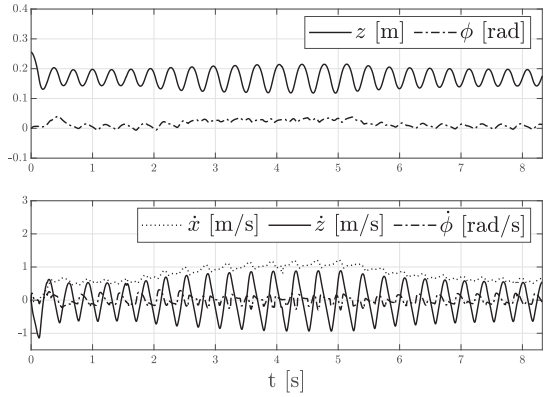

Fig. 10. Pose and velocity of the trunk during locomotion on the sagittal plane. Even if the dynamics of the segmented legs system is more complex than the model used for planning and control, stable trotting at the desired speed is robustly achieved. Moreover, the pitch angle deviations from the zero are kept remarkably small.

modes are natural evolutions of the system dynamics. More details about related strategies can be found in [25], [26].

Remark: A weighted pseudoinverse or QP approach (e.g. [28], [29]) can be used to realize the controller forces in (16) via joint actuation satisfying dynamic and kinematic constraints.

C. Example in Simulation

We perform simulations for an implementation of the actuated reduced-order elastic sagittal model to demonstrate that stable locomotion can be achieved with the proposed spring potential and control strategy. The model parameters are the presented in Table I. The resulting upright equilibrium configuration is $\boldsymbol{x}_\mathrm{b}^\mathrm{eq} = [0, 17.76\,\mathrm{cm}, 0]^\mathrm{T}$.

Fig. 3 presents the Eigenmanifold associated with the swing motion in the energy range 8.8 - 20 J. Following the planning strategy described in Section IV-B, the desired attack configurations are determined using (15). Fig. 6 presents the polynomial approximation of x_TD^d and z_TD^d as function of E^d within the studied energy range. The required attack angles and radial lengths of the legs for the flight phase are found with (5). The COM trajectories resulting from the simulations are depicted in Fig. 8, together with snapshots of the system. The simulations show that regular evolutions along the modal dynamics are achieved passively with the proposed controller, since $\boldsymbol{u}_\mathrm{p} = 0$ on the mode as shown in the plots of the control inputs in Fig. 8.

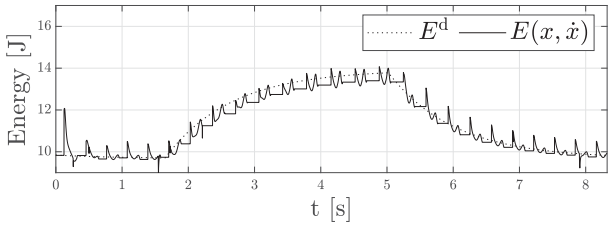

Fig. 11. Evolution of the mechanical energy showing good tracking of the desired value E^d which drives the speed of the gait.

VI. ANALYSIS OF ROBUSTNESS UNDER NON-IDEAL CONDITIONS

We present here a critical study of robustness and practical applicability of the proposed strategy. To this end, we developed a simulation of a lightweight quadrupedal robot with segmented legs presented in Fig. 9, which we implemented using the open-source software Gazebo. The simulation accounts for several unideal effects such as energetic losses due to impacts, friction cone at the feet, viscous friction in the joints, and legs with non-zero mass and inertias. The kinematic and inertial parameters are presented in Table II. We used Gazebo v11.0.0, with physics engine ODE and an update rate of 1 kHz. The controller is implemented in Simulink and runs synchronized with Gazebo at a fixed discrete rate of 1 kHz. We consider a friction cone with $\mu = 1$ at the feet, and viscous friction $0.025\,\mathrm{Nm\ s/rad}$ on all joints.

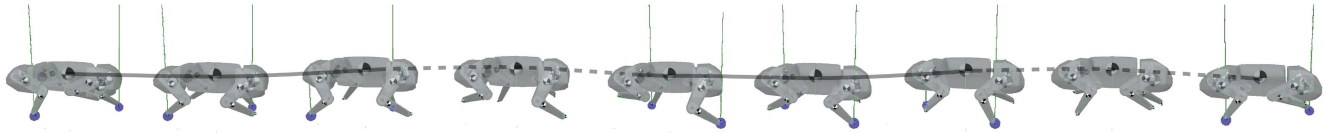

Fig. 12. Snapshots of the robot performing trotting in Gazebo. The blue dots denote contacts between the feet and the ground.

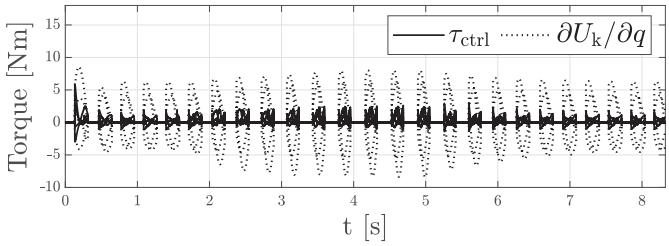

Fig. 13. Control input of the mode stabilizer versus the forces generated by the spring during the stance phase. The control torques are much lower than the spring forces: this indicates that the springs are being exploited and the locomotion's efficiency is increased.

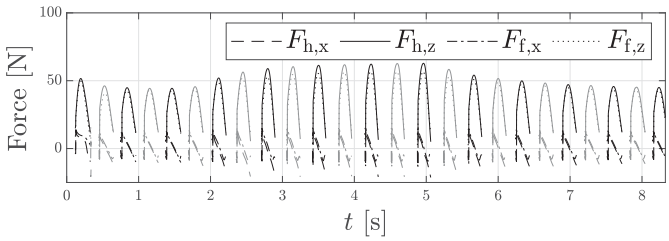

Fig. 14. Ground reaction forces at the feet generated by the spring forces during the modal oscillations in double support. The reaction forces refer to the hind and front diagonal pair of legs currently in contact, depicted in black for the front left and hind right, and in gray for the front right and hind left. The absence of forces corresponds to full flight phases, i.e., no leg is in contact with the ground..

TABLE II
PARAMETERS OF A ROBOT WITH SEGMENTED LEGS

	m [kg]	I_{yy} [kg · m^2]
Main Body	1.25	7e-3
Shoulder Link	0.636	1.5e-3
Thigh Link	0.124	5e-4
Shank Link	0.060	1e-4
Shoulder Distance	a	16.5 cm
Link Length	l	12 cm

A. Elastic Potential Design via Reduced Model

We approximate the inertia matrix of the trunk by locking the hips and neglecting the shank masses, resulting in $\boldsymbol{M}_b \approx \text{diag}(4.3, 4.3, 0.1)$. We consider the same potential U_{k} as in the simulations in Section V-C, but here we implement it with nonlinear springs collocated in parallel to the actuators on the joints $\boldsymbol{q}$. The spring potential is determined by writing the polar coordinates of the legs as function of $\boldsymbol{q}$ such that $U_{\text{k}} = U_{\text{k}}(\boldsymbol{q})$. In general, the spring force at one joint depends nonlinearly on other joint angles - these relationships can be well approximated with 5th to 7th degree polynomials.

To keep a safety margin, the planning of the attack configurations via (15) is evaluated with $\mu = 0.8$.

B. Flight Phase Control

A simple joint PD controller regulates the legs joints $\boldsymbol{q}_{\text{fl}}$ scheduled for the next stance phase to the attack configuration $\boldsymbol{q}_{\text{atk}} = \boldsymbol{q}_{\text{atk}}(\boldsymbol{p}_{\text{atk}})$

$$\boldsymbol{\tau}_{\text{fly}} = \boldsymbol{K}_{\text{p}}(\boldsymbol{q}_{\text{atk}} - \boldsymbol{q}_{\text{fl}}) - \boldsymbol{K}_{\text{v}}\dot{\boldsymbol{q}}_{\text{fl}} + \boldsymbol{f}_{\text{k}} \tag{19}$$

where $\boldsymbol{K}_{\text{p}}, \boldsymbol{K}_{\text{v}}$ are the proportional and derivative gains, and the additional compensation term $\boldsymbol{f}_{\text{k}} = \partial U_{\text{k}}(\boldsymbol{q})/\partial \boldsymbol{q}_{\text{fl}}$ makes $\boldsymbol{q}_{\text{atk}}$ a stable equilibrium. The flight PD controller has gains $\boldsymbol{K}_{\text{p}} = 4.5\boldsymbol{I}_4$, and $\boldsymbol{K}_{\text{v}} = 0.1\boldsymbol{I}_4$. The other two legs (that just detached from the ground) retract to a fixed configuration $\boldsymbol{q}_{\text{fix}} = [+1.2, -1.4, -1.0, +1.6]^{\text{T}}$ rad to avoid contact with the ground. The flight PD controller is also used during the stance phase on the two legs that are not in contact: these are regulated to $\boldsymbol{p}_{\text{atk}}$ for the next touch down, following a trajectory that avoids contact with the ground. To this end, the gains in (19) can be tuned to achieve sufficient precision within a longer transient.

C. Forward Trotting at Controllable Speed

The control strategy presented in Fig. 5 is used to excite and sustain a trotting gait. The mode controller drives the quadruped on modal oscillations at different energies in order to adjust the speed of the gait. A state machine keeps track of the current pair of legs in contact so that the locomotion is performed on alternate diagonal legs. The desired energy E^d is used to regulate the speed from a "slow" target $E_1 = 10\,\text{J}$ (corresponding to a forward velocity $\approx 0.5\,\text{m/s}$) to a "fast" target $E_2 = 14\,\text{J}$ ($\approx 1.1\,\text{m/s}$). The system is initialized at $z = 0.25\,\text{m}$, $x = \phi = 0$ and $\dot{x} = \dot{z} = \dot{\phi} = 0$. The stabilization and excitation of the mode is realized via the actuators of the legs in contact as $\boldsymbol{\tau}_{\text{st}} = \boldsymbol{J}_{\text{pq}}^{\text{T}}\boldsymbol{u}_{\text{p}}$, being $\boldsymbol{J}_{\text{pq}}$ the Jacobian mapping $\dot{\boldsymbol{p}} = \boldsymbol{J}_{\text{pq}}\dot{\boldsymbol{q}}_{\text{st}}$. The control gains are set as follow: $\boldsymbol{K} = 10I_3$, $\boldsymbol{D} = \text{diag}(13, 13, 30)$, and $\gamma = 10$.

The results of the simulation are presented in Fig. 10 and in Fig. 11, which depict the trunk trajectories and the evolution of the mechanical energy, respectively, and in Fig. 13, which compares the mode controller input profiles against the springs contributions. Additionally, snapshots of the simulations are presented in Fig. 12. We have included a supplementary MP4 video showing the simulations of the reduced model, and the Gazebo simulations of the quadruped performing trotting and pronking on flat ground at varying speed. This will be available at https://ieeexplore.ieee.org. The simulation shows that stable and regular trotting is robustly achieved within one locomotion cycle, and that the springs are exploited for the motion. Despite multiple sources of uncertainty and neglected dynamics, such as the nonzero leg mass, and impact and friction losses, the trunk attitude deviations are kept remarkably close to zero (max $1.5\,\text{deg}$ error, after the small initial transient) during the whole locomotion. Additionally, the approach proves to be robust against single-support phases, which are unaccounted for in the proposed planning method. The mode controller injects energy during the stance phase in order to sustain oscillations at the desired energetic level (Fig. 11). During the stance phase, the

forces generated by loading and releasing the springs contribute to as much as 4 times the magnitude of the input torques (Fig. 13): this indicates that the approach can be used to develop efficient gaits on future robots equipped with soft elastic elements.

D. Features and Limitations

While on the one hand a simple controller achieves quasi-passive locomotion by treating the problem in terms of nonlinear modal dynamics, on the other hand this design process introduces a few drawbacks.

Firstly, the COM trajectory resulting from the modal analysis requires discontinuous contact forces at touchdown to nominally perform the gait, as can be seen in Fig. 14. This is due to the fact that touch down and take off are performed while the springs (in particular the torsional ones) are still partially loaded. This introduces limitations for practical implementations, if the forces are not generated sufficiently fast. Furthermore, discontinuous forces may lead to additional energetic losses and to slip more easily on surfaces with low friction. Remarkably, however, all of these issues are greatly alleviated by considering lightweight legs. Secondly, the spring potential required for maintaining a constant attitude during the oscillations may result into a nonlinear function of the joint angles. The mechanical implementation could be then carried out by considering polynomial approximations, and simplifications may be possible by choosing appropriate legs kinematics. Thirdly, the use of a simplified model leads to locomotion gaits limited to sagittal motion. However, we believe that this restriction can be lifted and more complex gaits can be achieved by combining multiple nonlinear modes, and switching between them at suitable times.

VII. Conclusion

We presented a quasi-passive locomotion algorithm based on the excitation and stabilization of nonlinear modes for a sagittal quadruped robot endowed with soft springs. The spring potential is designed such that the rotational dynamics of the trunk is not excited along the modal oscillations. The method is validated in a simulation of a segmented leg elastic quadruped, which shows that the system trajectories evolve naturally along the desired Eigenmanifold for different energies. The proposed control architecture fully exploits the natural oscillations of the system during the stance phase. No feedback cancellations for template matching are required, not even gravity compensation. Future work will focus on experimental validation.

References

[1] C. Zhang, W. Zou, L. Ma, and Z. Wang, "Biologically inspired jumping robots: A comprehensive review," *Robot. Auton. Syst.*, vol. 124, 2020, Art. no. 103362.

[2] C. Della Santina, M. G. Catalano, and A. Bicchi, *Soft Robots*. Berlin, Heidelberg: Springer, 2021.

[3] F. Nan, H. Kolvenbach, and M. Hutter, "A reconfigurable leg for walking robots," *IEEE Robot. Automat. Lett.*, vol. 7, no. 2, pp. 1308–1315, Apr. 2022.

[4] A. Badri-Sprowitz, A. A. Sarvestani, M. Sitti, and M. A. Daley, "Birdbot achieves energy-efficient gait with minimal control using avian-inspired leg clutching," *Sci. Robot.*, vol. 7, no. 64, 2022, Art. no. eabg4055.

[5] M. Calisti, G. Picardi, and C. Laschi, "Fundamentals of soft robot locomotion," *J. Roy. Soc. Interface*, vol. 14, no. 130, 2017, Art. no. 20170101.

[6] N. Kashiri et al., "An overview on principles for energy efficient robot locomotion," *Front. Robot. AI*, vol. 5, 2018, Art. no. 129.

[7] J. Chen et al., "Towards the exploitation of physical compliance in segmented and electrically actuated robotic legs: A review focused on elastic mechanisms," *Sensors*, vol. 19, no. 24, 2019, Art. no. 5351.

[8] M. J. Pollayil et al., "Planning natural locomotion for articulated soft quadrupeds," in *Proc. Int. Conf. Robot. Automat.*, 2022, pp. 6593–6599.

[9] R. J. Full and D. E. Koditschek, "Templates and anchors: Neuromechanical hypotheses of legged locomotion on land," *J. Exp. Biol.*, vol. 202, no. 23, pp. 3325–3332, 1999.

[10] H. Geyer, A. Seyfarth, and R. Blickhan, "Compliant leg behaviour explains basic dynamics of walking and running," *Proc. Roy. Soc. B: Biol. Sci.*, vol. 273, no. 1603, pp. 2861–2867, 2006.

[11] Y. Gong et al., "Feedback control of a Cassie bipedal robot: Walking, standing, and riding a segway," in *Proc. IEEE Amer. Control Conf.*, 2019, pp. 4559–4566.

[12] M. Shahbazi, R. Babuška, and G. A. Lopes, "Unified modeling and control of walking and running on the spring-loaded inverted pendulum," *IEEE Trans. Robot.*, vol. 32, no. 5, pp. 1178–1195, Oct. 2016.

[13] M. A. Sharbafi, M. J. Yazdanpanah, M. N. Ahmadabadi, and A. Seyfarth, "Parallel compliance design for increasing robustness and efficiency in legged locomotion—proof of concept," *IEEE/ASME Trans. Mechatron.*, vol. 24, no. 4, pp. 1541–1552, Aug. 2019.

[14] C. Hubicki et al., "ATRIAS: Design and validation of a tether-free 3D-capable spring-mass bipedal robot," *Int. J. Robot. Res.*, vol. 35, no. 12, pp. 1497–1521, 2016.

[15] S. Collins, A. Ruina, R. Tedrake, and M. Wisse, "Efficient bipedal robots based on passive-dynamic walkers," *Science*, vol. 307, no. 5712, pp. 1082–1085, 2005.

[16] Z. Gan, T. Wiestner, M. A. Weishaupt, N. M. Waldern, and C. David Remy, "Passive dynamics explain quadrupedal walking, trotting, and tölting," *J. Comput. Nonlinear Dyn.*, vol. 11, no. 2, 2016, Art. no. 021008.

[17] A. Albu-Schaeffer and C. Della Santina, "A review on nonlinear modes in conservative mechanical systems," *Annu. Rev. Control*, vol. 50, pp. 49–71, 2020.

[18] C. Della Santina, D. Lakatos, A. Bicchi, and A. Albu-Schaeffer, "Using nonlinear normal modes for execution of efficient cyclic motions in articulated soft robots," in *Proc. Int. Symp.Exp. Robot.*, Springer, 2021, pp. 566–575.

[19] A. Sesselmann, F. Loeffl, C. Della Santina, M. A. Roa, and A. Albu-Schäffer, "Embedding a nonlinear strict oscillatory mode into a segmented leg," in *Proc. IEEE/RSJ Int. Conf. Intell. Robots Syst.*, 2021, pp. 1370–1377.

[20] D. Lakatos, W. Friedl, and A. Albu-Schäffer, "Eigenmodes of nonlinear dynamics: Definition, existence, and embodiment into legged robots with elastic elements," *IEEE Robot. Automat. Lett.*, vol. 2, no. 2, pp. 1062–1069, Apr. 2017.

[21] I. Poulakakis, E. Papadopoulos, and M. Buehler, "On the stability of the passive dynamics of quadrupedal running with a bounding gait," *Int. J. Robot. Res.*, vol. 25, no. 7, pp. 669–687, 2006.

[22] Z. Gan, Y. Yesilevskiy, P. Zaytsev, and C. D. Remy, "All common bipedal gaits emerge from a single passive model," *J. Roy. Soc. Interface*, vol. 15, no. 146, 2018, Art. no. 20180455.

[23] M. Raff, N. Rosa, and C. D. Remy, "Connecting gaits in energetically conservative legged systems," *IEEE Robot. Automat. Lett.*, vol. 7, no. 3, pp. 8407–8414, Jul. 2022.

[24] D. Calzolari, C. Della Santina, A. M. Giordano, and A. Albu-Schäffer, "Single-Leg forward hopping via nonlinear modes," in *Proc. IEEE Amer. Control Conf.*, 2022, pp. 506–513.

[25] C. D. Santina and A. Albu-Schaeffer, "Exciting efficient oscillations in nonlinear mechanical systems through eigenmanifold stabilization," *IEEE Control Syst. Lett.*, vol. 5, no. 6, pp. 1916–1921, Dec. 2021.

[26] C. D. Santina, D. Calzolari, A. M. Giordano, and A. Albu-Schäffer, "Actuating eigenmanifolds of conservative mechanical systems via bounded or impulsive control actions," *IEEE Robot. Automat. Lett.*, vol. 6, no. 2, pp. 2783–2790, Apr. 2021.

[27] F. Bjelonic, A. Sachtler, A. Albu-Schaffer, and C. Della Santina, "Experimental closed-loop excitation of nonlinear normal modes on an elastic industrial robot," *IEEE Robot. Automat. Lett.*, vol. 7, no. 2, pp. 1689–1696, Apr. 2022.

[28] M. Hosokawa, D. Nenchev, and T. Hamano, "The DCM generalized inverse: Efficient body-wrench distribution in multi-contact balance control," *Adv. Robot.*, vol. 32, pp. 1–15, 2018.

[29] G. Mesesan, J. Englsberger, G. Garofalo, C. Ott, and A. Albu-Schäffer, "Dynamic walking on compliant and uneven terrain using DCM and passivity-based whole-body control," in *Proc. IEEE-RAS 19th Int. Conf. Humanoid Robots*, 2019, pp. 25–32.